ACS Photonics

Article

Cite This: ACS Photonics 2017, 4, 2944-2951

pubs.acs.org/journal/apchd5

Form-Birefringence in ITO Thin Films Engineered by Ultrafast Laser Nanostructuring

Ausra Cerkauskaite,*[,†] Rokas Drevinskas,[†] Asi Solodar,[‡] Ibrahim Abdulhalim,[‡,§] and Peter G. Kazansky[†]

[†]Optoelectronics Research Centre, University of Southampton, Southampton, SO17 1BJ, United Kingdom

[‡]Department of Electro-Optics Engineering and The Ilse Katz Institute for Nanoscale Science and Technology, Ben Gurion University of the Negev, Beer Sheva 84105, Israel

[§]Singapore-HUJ Alliance for Research and Enterprise (SHARE), Nanomaterials for Energy and Energy-Water Nexus (NEW), Campus for Research Excellence and Technological Enterprise (CREATE), Singapore 138602

ABSTRACT: The field of surface nanostructuring is growing rapidly with the need to search for more advanced fabrication solutions. The major challenge is the lack of appropriate combination of time/cost efficient techniques and medium possessing the advantages of both flexibility and tunable optical properties. Here we demonstrate direct-write femtosecond laser nanostructuring of indium−tin-oxide thin film where the deep-subwavelength ripples with periodicity of down to 120 nm are realized originating the form birefringence ($|\Delta n| \approx 0.2$), which is 2 orders of magnitude higher than the commonly observed in uniaxial crystals or femtosecond laser nanostructured fused quartz. The demonstrated nanoripples with its continuously controlled space-variant orientation lead to the high density two-dimensional printing of flat optical elements. The technique can be extended to any highly transparent films that support laser-induced periodic surface structures, and can be effectively exploited for the integration of polarization sensitive modifications into multidimensional optical data storage.

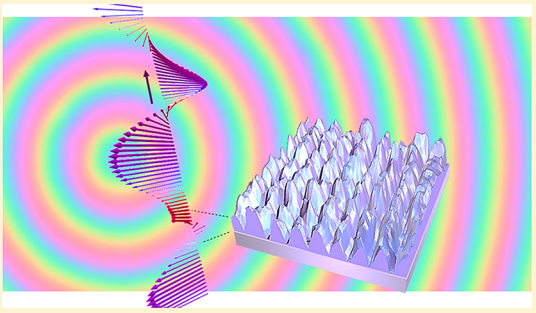

KEYWORDS: *form birefringence, laser material processing, femtosecond pulses, geometric phase, optical data storage*

Recently ultrafast laser processing of transparent materials has made promising progress toward the realization of high performance three-dimensional microelements, flat optics, and optical data storage.[1−4] The main advantage of using femtosecond pulses for direct laser writing is that they can rapidly deposit energy in solids with high precision. The light is absorbed and the optical excitation ends before the surrounding lattice is perturbed, which results in highly localized modification without collateral material damage.[5,6] Under certain processing conditions, multipulse irradiation causes the material to reorganize into laser-induced periodic surface structures (LIPSS) at micro- and nanoscale, which was observed on virtually any type of media such as metal, semiconductor, dielectric solids, and thin films,[7] including indium tin oxide (ITO) film.[8−11]

Almost two decades ago it was demonstrated that femtosecond laser pulses focused inside silica glass can lead to self-assembled nanogratings,[12,13] which exhibit birefringence comparable to quartz crystals.[14] Later, this anisotropy in silica was engineered to surface nanogratings showing a 3-fold birefringence increase.[15] Although the laser-induced birefringence is high enough for realization of various functional elements, the resultant thickness of nanostructures limits its performance in flat optics.[2] Recent experimental investigations revealed 2 orders of magnitude higher birefringence in amorphous silicon[16,17] and silicon carbide[18] films, suggesting that the high-refractive-index materials could be used for fabricating anisotropic surfaces. However, high intrinsic losses of materials and low quality of induced LIPSS prevent the realization of efficient optical elements. This challenge can be overcome by using materials with a transparency window in the visible spectrum, and achieving precise direct-writing of high-frequency nanostructures.

ITO substrates have been widely used for optoelectronic devices such as solar cells, flat panel displays, thin-film photovoltaics, organic light emitting diodes and smart windows due to their high transparency and excellent conductivity caused by its highly degenerate behavior as an n-type semiconductor with a large band gap of around 3.5 to 4.3 eV.[19,20] Here we propose a direct-write ultrafast laser nanostructuring of ITO thin films as an alternative method of printing highly transparent polarization sensitive elements. The observed patterns with the subwavelength modulation (period down to 120 nm) of the material with refractive index changing from $n \approx 1.9$ for ITO to $n \approx 1$ for grooves exhibit an enhanced form birefringence ($|\Delta n| \approx 0.2$), which is almost 2 orders of

Received: September 18, 2017
Published: October 24, 2017

DOI: 10.1021/acsphotonics.7b01082
ACS Photonics 2017, 4, 2944−2951

magnitude higher than in femtosecond laser nanostructured fused quartz. The control of orientation and strength of nanostructuring is achieved within a submicron thickness realizing the fabrication of space-variant polarization sensitive optical elements, polarization, and intensity multiplexed optical data storage.

MATERIALS AND METHODS

Experiments are carried out with 145 ± 10 nm thick ITO film deposited on float glass by sputtering, prepared by Thin Film Devices (TFD Inc., California). Samples are irradiated with ytterbium-doped potassium gadolinium tungstate (Yb: KGW) based mode-locked regenerative amplified femtosecond laser system PHAROS (Light Conversion Ltd.) operating at a wavelength of 1030 nm (photon energy ~ 1.2 eV) with the repetition rate of 500 kHz and the pulse duration tuned in the range of 0.4−1 ps. The laser beam is focused via a 0.03 NA, 0.16 NA and 0.65 NA objective lenses on the surface of sample, which is mounted on a XYZ linear air-bearing translation stage (Aerotech Ltd.). Local orientation of induced nanostructures, that is, the azimuth of slow-axis of laser-induced form birefringence, is continuously controlled by rotating the half-wave plate mounted on the motorized rotational stage before the objective lens (Figure 1), where 0°/90° orientations are

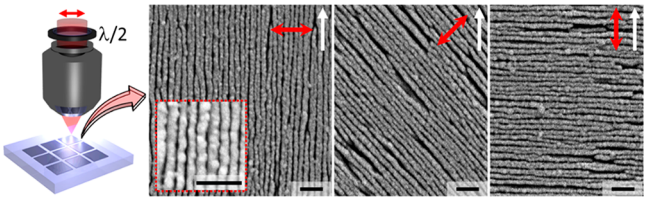

Figure 1. SEM top view images of femtosecond laser nanostructured ITO film. The orientation (red arrows) of the linearly polarized incident laser beam was controlled by rotating the half-wave plate ($\lambda/2$) placed before the objective. White arrows indicate the writing direction. Processing conditions: 0.68 μJ pulse energy, 0.4 ps pulse duration, 500 μm^{-1} pulse density, focusing via 0.03 NA lens, 1 mm/s scanning speed. Scale bar is 500 nm.

perpendicular/parallel to the writing direction. For scanned modification, the sample translation speed varies from 1 to 0.1 mm/s, which corresponds to 500−5000 μm^{-1} pulse density. The interline writing distance of 4 μm, 1 and 0.5 μm, and pulse energy less than 1, 0.05, and 0.03 μJ are fixed for each objective lens with 0.03, 0.16, and 0.65 NA, respectively.

The nanostructured ITO is optically characterized using the VIS/NIR microspectrometer CRAIC (integrated in Olympus microscope BX51). The laser-induced birefringence, that is, retardance and its slow axis, is analyzed and visualized with the quantitative birefringence measurement system (CRi Abrio; Olympus BX51) operating at 546 nm. The imaging of laser-induced structures is performed with a scanning electron microscope (SEM) Zeiss Evo50 and optical transmission microscope Olympus BX51.

RESULTS AND DISCUSSION

At the pulse energies slightly above the ablation threshold, the ITO film is modified along its depth organizing into periodic structure that is qualitatively dependent on the laser material processing conditions. Under the processing conditions used to scan large area of ITO film (Figure 1), the nanostructure with periodicity of ~120 nm and duty cycle of roughly 10−20% of the nanogrooves oriented perpendicular to the incident laser polarization is formed. Such high spatial frequency structure has period significantly smaller than the irradiation wavelength ($\sim\lambda/9$), and in general is observed after modification by ultrashort laser pulses under tens to thousands of laser pulses per irradiation spot. The origin of induced structures is still controversially discussed in literature considering the preseeding and accumulation effects, near-field enhancement, interference between surface waves and incident laser beam, self-organization of nanostructures during the relaxation of a highly nonequilibrium surface,[5,21−27] as well as the subsequent transformation of ITO atomic lattice may possibly be involved.[8]

The nanostructured ITO might be considered as a metamaterial that possesses the properties capable of manipulating electromagnetic waves. Depending on the modification conditions, the induced structure diverges from highly patterned nanoripples to fully ablated glass substrate, changing the resultant quality and thickness of the film. Thus, it is very important to operate close to the modification threshold in order to produce debris- and fracture-free nanostructures with the elevated optical properties.

The internal transmittance of pristine ITO film is expected to be more than 99%, where the absorption is less than 1%. Thus, the measured transmission spectra and optical losses are mainly governed by the surface reflections. After the laser irradiation, the overall transmission in the visible spectral range of >87% was measured (ITO band gap ~ 4 eV[19]). Moreover, the nanostructured film exhibits the increase of optical transmission by 5% at 750 nm wavelength giving the total transmission value of 93% (Figure 2a).

The light wave in such subwavelength structure behaves the same way as that in the uniaxial anisotropic material with negative form birefringence.[28−31] Propagation of optical waves in such periodic media can thus be described by the effective refractive indices originating from the effective-medium theory.[28] This means that the electric field oscillating along (TE mode) and perpendicular (TM mode) to the grooved medium obtain a different amount of phase shift. As a result, the phase retardation (φ) of transmitted light can be directly determined by the thickness (d) of the nanoripples and its possessed form birefringence ($\Delta n = n_{TE} - n_{TM}$):

$$\varphi = d \cdot \Delta n \quad (1)$$

The resulting form-birefringence can exceed the value of natural birefringence of uniaxial crystals, and is usually designed by controlling the refractive index, periodicity, and duty cycle of the periodic nanostructures. Assuming that the nanoripple is uniform along its depth, the value of achieved birefringence can be estimated from the measured retardance value and film thickness.

The dispersion analysis of retardance performed in the spectral region from 500 to 750 nm reveals a chromatic behavior of the imprinted elements (Figure 2a). The retardance value varies from 33 to 45 nm, and linearly decreases with the wavelength increase corresponding to ~0.18π rad phase retardation at 500 nm wavelength and ~0.09π rad phase retardation at 750 nm wavelength.

A commercial-grade simulator based on the finite-difference time-domain (FDTD) method is used to perform the numerical calculations of electric field propagation.[32] A broadband plane wave source is incident on the ITO film from the glass side, and the transmission spectrum is measured by a numerical monitor from the air side. A 2D monitor is used

DOI: 10.1021/acsphotonics.7b01082
ACS Photonics 2017, 4, 2944−2951

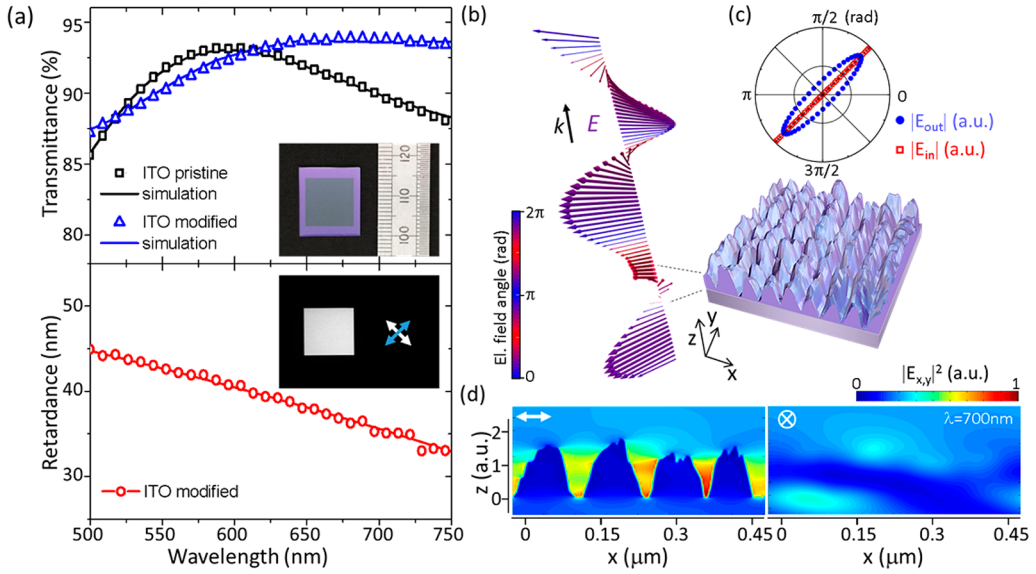

Figure 2. Optical characterization of nanostructured ITO film. Processing conditions: 0.68 μJ pulse energy, 0.4 ps pulse duration, 500 μm^{-1} pulse density, focusing via 0.03 NA lens, 1 mm/s scanning speed. (a, top) Measured (open symbols) and simulated (solid line) optical transmission spectra of pristine and modified ITO thin film. The illumination was unpolarised. Inset shows a large-scale 12 × 12 mm scanned area. (a, bottom) Measured (open circles with solid line) retardance spectrum of modified ITO. Inset represents the large-scale 12 × 12 mm modified region imaged under crossed polarized light. White and blue arrows indicate the polarization orientation before the sample and after the analyzer placed before the detector. (b) Simulated electric field propagation (λ = 700 nm) through the 3D structure modeled rendering SEM image (Figure 1, left). The color of the vectors represents its angular orientation in space. (c) Distribution of input and output magnitude of the electric field vectors plotted in polar coordinates. The magnitude is normalized to the source (input) magnitude. (d) Electric field intensity distribution for two orthogonal polarizations: perpendicular and parallel polarization to the orientation of laser-induced nanoripples. Thickness of the numerically simulated structures is normalized to the thickness of pristine ITO film.

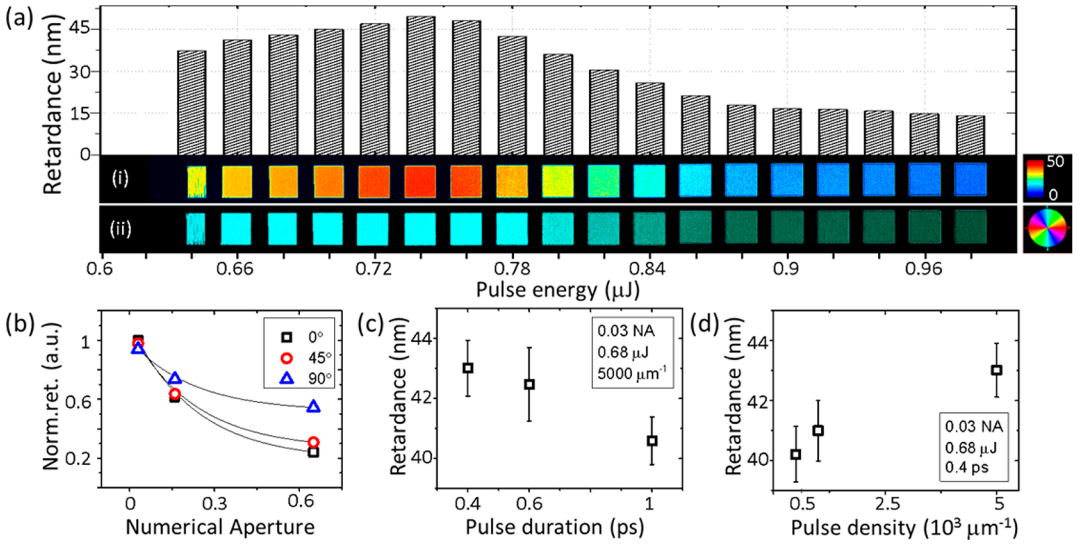

Figure 3. Form-birefringence of ultrafast laser nanostructured ITO film. (a) Laser-induced retardance as a function of pulse energy. The film was processed by 0.4 ps laser pulses with polarization oriented perpendicular to the writing direction (top-down) and pulse density of 5000 μm^{-1} at 0.1 mm/s scanning speed, under weak focusing conditions (0.03 NA). (i) Retardance and its corresponding (ii) slow axis orientation images of squares (0.25 × 0.25 mm) printed at various pulse energies. (b) Normalized retardance dependence on different focusing conditions and various orientations of incident linearly polarized laser beam. The pulse energy was set to 0.74 μJ (0.03 NA), 0.04 μJ (0.16 NA), and 0.014 μJ (0.65 NA). (c) Retardance dependence on pulse duration and (d) pulse density, at a fixed processing conditions.

to capture the E-field distribution as a function of wavelength. The refractive index spectra for ITO is taken from literature.[33] The corresponding total electric field distribution is obtained simulating its propagation through the 3D structure reconstructed rendering the SEM image (Figure 2b). The simulated transmission spectra for pristine and modified ITO are in a good agreement with the spectra observed experimentally (Figure 2a). However, in order to fit the measured spectra, the thickness of the 3D structure has to be increased by a factor of 1.5 (Figure 2d). This suggests that under the conditions slightly above the modification threshold the material is periodically pushed away from the initial position forming the nanogrooves and a greater thickness ITO. From eq 1, assuming that the

DOI: 10.1021/acsphotonics.7b01082
ACS Photonics 2017, 4, 2944−2951

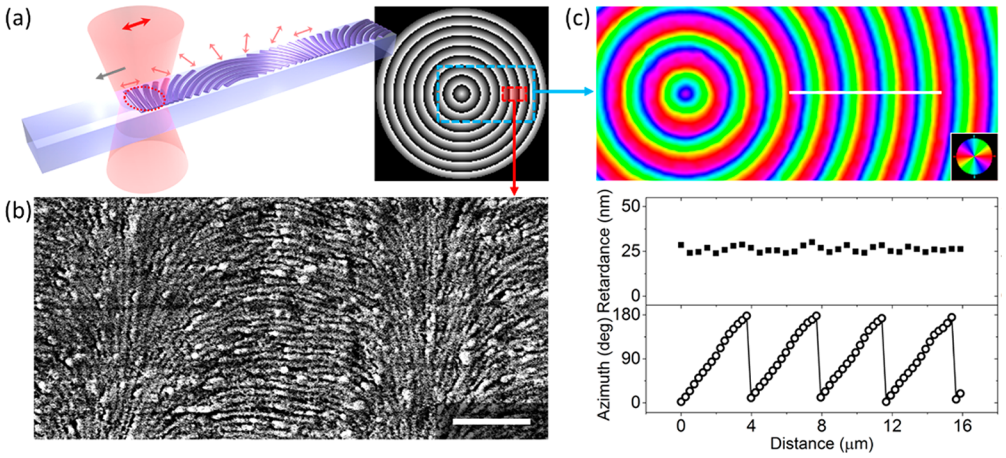

Figure 4. Optical element designed as a polarization sensitive circular grating. (a) Schematics of fabrication of spatially variant surface ripples, and the calculated phase pattern of the element in grayscale. The period and pixel-to-pixel distance were fixed to 4 and 0.4 μm, respectively. Red arrows represent the local orientation of incident linear polarization. Gray arrow shows the direction of scanning. (b) SEM image of the induced nanostructures. Scale bar is 1 μm. (c, top) Azimuth image of the slow-axis of the imprinted pattern; (c, bottom) the profile (white line in the top image) of retardance and azimuth of the slow-axis extracted from the birefringence measurements performed at 546 nm wavelength. Pseudo colors represent the orientation of the slow axis.

average thickness is around 200 nm, laser-induced birefringence as high as $\Delta n \approx -0.2$ is achieved.

At a fixed point in XY space, the linearly polarized (45°) input electric field E after passing the ITO nanoripples traces out an ellipse in the $X-Y$ plane (Figure 2b,c). The polarization is rotated from linear to elliptical with the axes ratio of $|E|_{\pi/4}/|E|_{-\pi/4} \approx 0.17$. Then the retardance can be expressed as

$$\varphi = a \cos(I_{pp} - I_{cp}/I_{pp} + I_{cp}) \times \lambda/2\pi \quad (2)$$

where I_{pp} and I_{cp} are the electric field intensities for polarizations oriented parallel and perpendicular (cross-polarized) to the input polarization. The estimated retardance value at 700 nm wavelength is slightly higher than 35 nm, which correlates well with the measured retardance plotted in Figure 2a.

In addition to the optical transmission, the simulations confirm that the fabricated structure behaves similar to a wire grid polarizer or an array of subwavelength slits,[34] when the light polarized parallel (TE) to the nanogrooves does not feel the structure and is transmitted or reflected almost in the same way as in pristine film, and the light polarized perpendicular (TM) shows the enhanced interaction with the structure (Figure 2d). In this case, the excited groove cavity modes are expected to increase the overall optical transmission.

When designing high performance polarization sensitive elements by laser direct writing, it is important to ensure the optimum processing condition for imprinted nanoripples. In general, the ultrafast laser nanostructuring is a multipulse induced process,[35,36] and the local fields as well as the final patterns both for scanning and stationary irradiation are always affected by the previously induced structure. Thus, the effect of such accumulative processes is strongly dependent on the deposited pulse energy, focusing conditions, pulse density and pulse duration. Under weak focusing conditions (0.03 NA) and pulse energy of around 0.64 μJ (Figure 3a), the film is modified along its depth and periodically organized into nanoripples oriented perpendicular to the laser beam polarization. The anisotropic structure with highest transmission is produced reaching the retardance value of ~37 nm, which is maximized to 50 nm at 0.74 μJ pulse energy. The further energy increase is accompanied by the removal of ITO leading to the retardance decrease. As a result, the retardance value drops by 70% to 15 nm at 0.9 μJ. Qualitatively, the same behavior of retardance as a function of pulse energy is observed under all processing conditions including tight focusing of up to 0.65 NA, pulse durations from 400 fs to 1 ps, and by an order of magnitude lower pulse densities.

The retardance value is highly dependent on the focusing conditions (Figure 3(b)). The transition from 0.03 to 0.65 NA causes almost 80% retardance drop for polarization perpendicular to writing direction, and 40% for polarization parallel to writing direction. The polarization effect comes from *s*- and *p*-polarizations, when the light polarized perpendicular to the modification front (*p*-polarization) is transmitted into the film more effectively. The weak dependence on pulse duration, when the value of retardance changes only by 6%, that is, from 43 to 40.5 nm, with the variation of pulse duration from 0.4 to 1 ps at a fixed pulse energy, is observed (Figure 3c). However, if the pulse duration is increased to 5 ps, the modification threshold changes drastically exceeding the energy range indicated in Figure 3a. Both for scanning and stationary cases the nanoripples formation requires multipulse irradiation, thus the final modification is always influenced by the structure induced within the first pulses. If the pulse energy is slightly above the nanostructuring threshold but is not sufficient to remove the film, the gradual growth of retardance is initiated within every delivered pulse. Under certain scanning conditions (Figure 3d), 10-fold increase in pulse density leads to the increase of retardance value only by 10%, indicating the saturation of the nanostructuring process.

Flat Optics. Due to the high spatial frequency of ripples with period of $\sim\lambda/9$, the subwavelength resolution of continuously controlled space-variant patterns, referred to as geometric phase optical elements, can be designed (Figure 4). The polarization sensitive circular (blazed) grating with period of 4 μm is fabricated continuously translating the sample with linear speed of 0.1 mm/s and modulating the input linear polarization of laser beam from 0° to 180°. The high-precision sample translation with the repeatability of 50 nm along with the polarization modulation of up to 250 × 2π rad/s is ensured.

DOI: 10.1021/acsphotonics.7b01082
ACS Photonics 2017, 4, 2944−2951

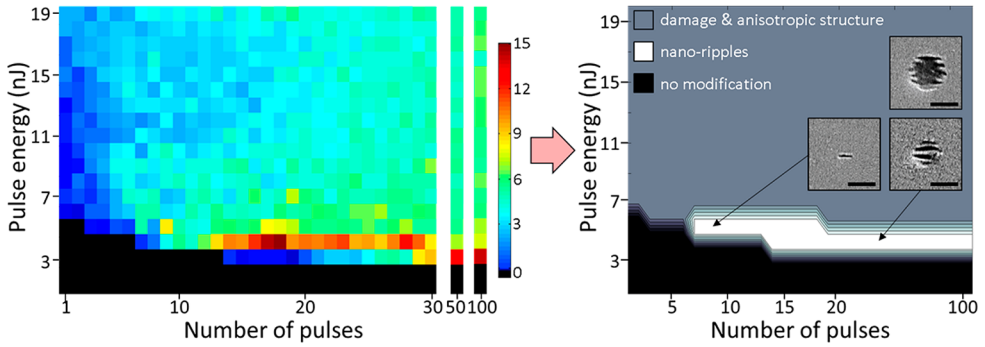

Figure 5. Retardance map (left) as a function of pulse energy and number of pulses extracted from the matrix of dots printed in ITO film. (right) Schematic map of the threshold energies with its structuring regimes. Insets show the SEM images of the laser-induced ripples and damage with/without anisotropic structure. Scale bar is 1 μm. Black region indicates the conditions when the modification was not observed. Processing conditions: 0.4 ps pulse duration, 0.65 NA lens. Color bar is a linear retardance scale in nm.

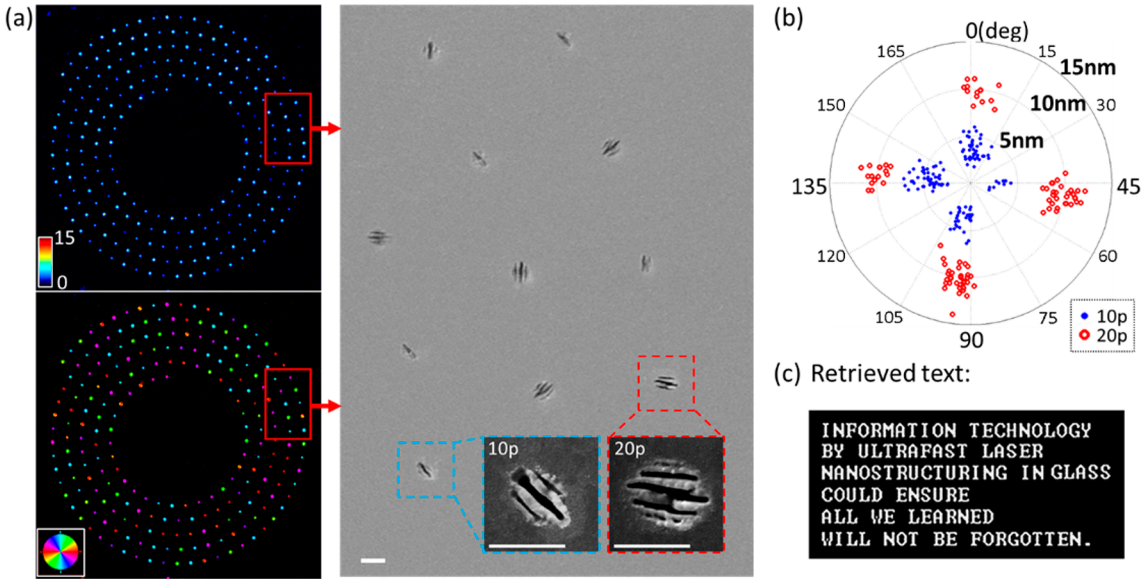

Figure 6. Polarization and intensity multiplexed data storage. (a) Images of the (left) retardance and slow axis orientation of imprinted dots, and (right) the corresponding enlarged area under SEM. Insets represent structures induced using 10 and 20 pulses at a fixed 4 nJ pulse energy, 0.4 ps pulse duration, and focusing via 0.65 NA objective lens. Color bar is a linear retardance scale in nanometers. Pseudo colors represent the orientation of the slow axis. Scale bar is 1 μm. (b) Distribution of the readout data points depending on the slow axis orientation and the level of the retardance. Blue and red points indicate the modification induced by 10 and 20 pulses, respectively. (c) Text retrieved from the readout data points.

The phase pattern calculated in grayscale is used as a reference for mapping the local input polarization orientation, where 0 value corresponds to 0° and 255 value corresponds to 180° (Figure 4a). The interline writing and pixel-to-pixel distance is fixed to 0.4 μm. Pulses with duration of 0.4 ps and energy of 4 nJ are focused via 0.65 NA objective lens.

The fabricated element relies on the space-variant polarization-state manipulation, and the resultant phase-shift magnitude (ϕ) of the input circular polarization is solely defined by the nanoripples azimuth (A) of the slow axis, that is, $\phi(x,y) = \pm 2A(x,y)$.[37] Depending on the handedness of the input circular polarization, the element possesses phase profile of a concave or convex axicon lens.

For an incident plane wave with the polarization state $|E_{in}\rangle$ the resulting field generated by the grating would be $|E_{out}\rangle = \eta_E|E_{in}\rangle + \eta_R e^{i2A(x,y)}|R\rangle + \eta_L e^{-i2A(x,y)}|L\rangle$,[38] where the $\eta_E = 1/2(t_x + t_y e^{i\varphi})$, $\eta_R = 1/2(t_x - t_y e^{i\varphi})\langle E_{in}|L\rangle$ and $\eta_L = 1/2(t_x - t_y e^{i\varphi})\langle E_{in}|R\rangle$ are the complex field efficiencies with $\langle E_{in}|R,L\rangle$ as an inner product of the left-handed $|L\rangle$ and right-handed $|R\rangle$ circular polarizations, φ is the retardance of the imprinted element, and $t_{x,y}$ are the transmission coefficients for light polarized perpendicular and parallel to the optical axis. The imprinted gratings with $t_{x,y} \approx 0.9$ (Figure 2a) and $\varphi \approx 0.1\pi$ (Figure 4c) at 546 nm wavelength is expected to diffract around 0.022 of the total incident light intensity, while the remaining intensity would be nondiffracted or scattered. The efficiency expressed as a ratio of first order diffracted light and total transmitted light, $\eta_{1st} = E_{1st}/E^{(T)}_{total}$, would be ~2.5%. The efficiency of elements can be drastically increased by having retardance close to half-wave. In this case, the processing of approximately 1.5 μm thick ITO films has to be performed. The retardance value of the printed element with the corresponding azimuth density possesses the standard deviation of around 1.6 nm, and azimuth is slightly deviated from the linear profiles (Figure 4b, bottom), which is mainly caused by the misalignment of the polarization optics. Despite the low efficiency of the designed element, the handedness of the diffracted circularly polarized beam is flipped, and the polarization filtering could be applied in order to completely eliminate the nondiffracted light.

DOI: 10.1021/acsphotonics.7b01082
ACS Photonics 2017, 4, 2944−2951

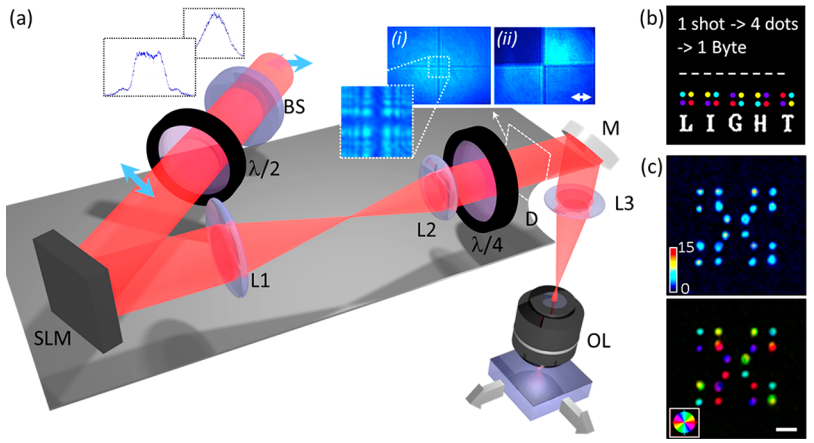

Figure 7. Parallel recording of polarization multiplexed data using a spatial light modulator (SLM), under conditions 10 pulses at a fixed 0.38 μJ total pulse energy, 0.4 ps pulse duration, and focusing via 0.65 NA objective lens. (a) Sketch of ultrafast laser direct writing setup: Gaussian to flat-top beam shaper (BS), half-wave plate ($\lambda/2$), SLM, imaging lenses (L1−3), quarter-wave plate ($\lambda/4$), removable CCD detector (D), mirror (M), and objective lens (OL). Blue arrows indicate the input polarization. Insets show the intensity distribution of the beam imaged (i) without and (ii) with linear analyzer on the detector. (b) The principle of data recording: within one shot (voxel) four dots with independent polarization are imprinted allowing to store 1 Byte of information. (c) Polarization sensitive imaging of recorded "LIGHT". (top) Retardance map of the imprinted structures with its corresponding (bottom) slow axis orientation. Color bar is a linear retardance scale in nanometres. Pseudo colors represent the orientation of the slow axis. Scale bar is 10 μm.

Polarization and Intensity Multiplexed Data Storage. The quantitative and qualitative analysis of the single dots induced under stationary printing conditions have been performed (Figure 5). The matrix of dots is printed using 1−100 pulses with pulse energy of up to 0.02 μJ and pulse duration of 0.4 ps focused via 0.65 NA lens. If the energy of the first pulse is sufficient to remove the ITO film (>5 nJ), the symmetric crater shape structure is produced. The observed threshold energy is roughly 10× lower than in silica glass under the similar processing conditions.[35] The subsequent irradiation does not affect the radius of the ablated region, but generates the nanoripples located at periphery. If the energy of the pulse is in the range of approximately 3−4 nJ, the first pulse does not induce any observable modification. However, due to the accumulative processes the single nanogroove with consistent slow axis orientation perpendicular to the incident laser beam polarization is formed within 7−14 pulses. The size and number of grooves increase with the subsequent pulses.

Based on the quantitative birefringence measurements, retardance value is maximized at around 15 nm after delivering 100 pulses with 3 nJ pulse energy, and 18 pulses with 4 nJ pulse energy. The retardance decreases within the further irradiation as the central region is removed. As a result, the induced nanoripples are always accompanied by the ablated central region, and the measured retardance value drops by 50% within 100 pulses at the pulse energy of 4 nJ. Therefore, the mapped retardance (Figure 5, left) can be divided into three different regions (Figure 5, right): (1) no modification when the pulse energy and number of pulses are below the modification threshold; (2) highly organized nanoripples; and (3) damage or ablated structures followed by the nanoripples.

The laser processing conditions used to record digital data are chosen based on the Figure 3 and Figure 5. The pulse energy is kept slightly above the modification threshold in order to attain the high quality of induced nanoripples, that is, transmission higher than 85% and retardance up to 15 at 546 nm wavelength. In the case of single dot printing (Figure 6), 10 and 20 pulses with the energy of 4 nJ, and for parallel recording (Figure 7), 10 pulses with the energy of 0.38 μJ are used. The increase of threshold energy for parallelized processing is caused by the intensity spread out in the image plane when only a fraction of the energy located at the hot-spots in the central part of the pattern focused on the ITO film is absorbed to induce the modification (Figure 7a,i). If the spot size of the input beam is reduced enough to have a sufficient intensity in the central part of the pattern, the single dot modification (i.e., single voxel) with the merged regions of four independent slow axis orientations could be produced.

For parallelized recording the single pass spatial light modulator (SLM; Hamamatsu Photonics) and fixed quarter-wave plate approach, similar reported elsewhere,[39,40] is implemented (Figure 7a). For input linear polarization aligned 45° to the direction of liquid crystal optic axis, the incident light experiences phase retardation from 0 to 2π radians depending on the input pixel value in 8-bit grayscale image (600 × 800 pixels). The resultant beam passing the quarter-wave plate acquired linear polarization of any orientation from 0° to 180° with ∼0.7° resolution. Thus, the generated SLM pattern of four segments with four different grayscale values is imaged on the ITO film using f_{1-3} = 400, 125, and 200 mm lenses and 0.65 NA (f = 2.8 mm) objective.

For single beam irradiation (Figure 6), the data is encoded into four different orientations and two different levels of strength of nanostructuring. Thus, each birefringent dot holds 3 bits of information, and therefore 2 dots represent one character. In this case, 64 different characters can be encoded. In parallel recording case (Figure 7a,b), four independent polarizations give the ability to store 1 Byte of information within one shot, which corresponds to one 8-bit character.

The information is retrieved combining two sets of data provided by raw birefringence measurements (Figure 6a and Figure 7b). Analyzing the distribution of the readout data points (Figure 6b), the retardance value from 2 to 7 nm for lower level and from 7.5 to 14 nm for higher level, and the mean values of slow axis of around 2°, 47°, 92°, and 137° with maximum deviation of ±8° are obtained. Both for single dot and parallel recording the 100% readout is demonstrated

DOI: 10.1021/acsphotonics.7b01082
ACS Photonics 2017, 4, 2944−2951

(Figure 6c and Figure 7c), with no additional error corrections applied.

The writing capacity depends on the bits per dot density and the planar compaction of modifications. Under the laser processing conditions discussed in this work, the separation between dots can be reduced down to 1 μm (Figure 6a). Furthermore, the slow axis analysis shows that six extra polarization orientations without the levels overlapping could be added to increase the bits per dot density (Figure 6b). This would result to more than 4 bits per modification what potentially leads to the overall capacity of around 6 GB per 120 mm size single-layer disc. The recording speed (6 B/s) is mainly limited by the hardware (e.g., characteristic rise/fall time of SLM limits the speed to 6 Hz), and therefore is out of the scope in our study. However, the successful demonstration of parallel processing given in Figure 7 clearly shows the feasibility of implementing fast hologram-free polarization multiplexed data recording. The multiplication of four active grayscale segments to full matrix of independently controlled SLM pixels could increase the recording speed by at least several orders.

CONCLUSION

The femtosecond laser direct nanostructuring of indium−tin-oxide results in highly organized surface ripples with form birefringence of $|\Delta| \approx 0.2$. Under energies slightly above the modification threshold, the transmission of nanostructured ITO exceeds the transmission of pristine film. Such engineered optical properties of the material could be implemented in fabrication of polarization sensitive elements and optoelectronic devices. The full control of orientation and strength of nanostructuring gives the potential of technique to be used in fabricating high-density flat optics, polarization, and intensity multiplexed data recording that add extra dimensions leveraging the capacity of conventional optical data storage by at least four times.

AUTHOR INFORMATION

Corresponding Author

*E-mail: ac1d14@soton.ac.uk.

ORCID

Ausra Cerkauskaite: 0000-0002-2476-7797

Asi Solodar: 0000-0001-6501-2000

Funding

Engineering and Physical Sciences Research Council (EPSRC) (EP/M029042/1).

Notes

The authors declare no competing financial interest.

ACKNOWLEDGMENTS

The data for this work is accessible through the University of Southampton Institutional Research Repository (DOI: 10.5258/SOTON/D0050). This research is partially supported by grants from the National Research Foundation, Prime Minister's Office, Singapore under its Campus of Research Excellence and Technological Enterprise (CREATE) programme.

REFERENCES

(1) Malinauskas, M.; Zukauskas, A.; Hasegawa, S.; Hayasaki, Y.; Mizeikis, V.; Buividas, R.; Juodkazis, S. Ultrafast Laser Processing of Materials: From Science to Industry. *Light: Sci. Appl.* **2016**, *5*, 16133.

(2) Drevinskas, R.; Kazansky, P. G. High-Performance Geometric Phase Elements in Silica Glass. *APL Photonics* **2017**, *2*, 66104.

(3) Zhang, J.; Čerkauskaitė, A.; Drevinskas, R.; Patel, A.; Beresna, M.; Kazansky, P. G. Eternal 5D Data Storage by Ultrafast Laser Writing in Glass. In *Laser-based Micro- and Nanoprocessing X*; Klotzbach, U., Washio, K., Arnold, C. B., Eds.; SPIE, 2016; p 97360U.

(4) Li, X.; Cao, Y.; Tian, N.; Fu, L.; Gu, M. Multifocal Optical Nanoscopy for Big Data Recording at 30 TB Capacity and Gigabits/second Data Rate. *Optica* **2015**, *2*, 567.

(5) Sundaram, S. K.; Mazur, E. Inducing and Probing Non-Thermal Transitions in Semiconductors Using Femtosecond Laser Pulses. *Nat. Mater.* **2002**, *1*, 217−224.

(6) Gattass, R.; Mazur, E. Femtosecond Laser Micromachining in Transparent Materials. *Nat. Photonics* **2008**, *2*, 219−225.

(7) Bonse, J.; Krüger, J.; Höhm, S.; Rosenfeld, A. Femtosecond Laser-Induced Periodic Surface Structures. *J. Laser Appl.* **2012**, *24*, 42006.

(8) Cheng, C. W.; Shen, W. C.; Lin, C. Y.; Lee, Y. J.; Chen, J. S. Fabrication of Micro/nano Crystalline ITO Structures by Femtosecond Laser Pulses. *Appl. Phys. A: Mater. Sci. Process.* **2010**, *101*, 243−248.

(9) Cheng, C. W.; Lee, I. M.; Chen, J. S. Femtosecond Laser Processing of Indium-Tin-Oxide Thin Films. *Opt. Lasers Eng.* **2015**, *69*, 1−6.

(10) Afshar, M.; Straub, M.; Voellm, H.; Feili, D.; Koenig, K.; Seidel, H. Sub-100 Nm Structuring of Indium-Tin-Oxide Thin Films by Sub-15 fs Pulsed near-Infrared Laser Light. *Opt. Lett.* **2012**, *37*, 563.

(11) Hasegawa, S.; Shiono, K.; Hayasaki, Y. Femtosecond Laser Processing with a Holographic Line-Shaped Beam. *Opt. Express* **2015**, *23*, 23185.

(12) Kazansky, P.; Inouye, H.; Mitsuyu, T.; Miura, K.; Qiu, J.; Hirao, K.; Starrost, F. Anomalous Anisotropic Light Scattering in Ge-Doped Silica Glass. *Phys. Rev. Lett.* **1999**, *82*, 2199−2202.

(13) Shimotsuma, Y.; Kazansky, P. G.; Qiu, J.; Hirao, K. Self-Organized Nanogratings in Glass Irradiated by Ultrashort Light Pulses. *Phys. Rev. Lett.* **2003**, *91*, 247405.

(14) Bricchi, E.; Kazansky, P. G. Extraordinary Stability of Anisotropic Femtosecond Direct-Written Structures Embedded in Silica Glass. *Appl. Phys. Lett.* **2006**, *88*, 111113−111119.

(15) Drevinskas, R.; Gecevičius, M.; Beresna, M.; Bellouard, Y.; Kazansky, P. G. Tailored Surface Birefringence by Femtosecond Laser Assisted Wet Etching. *Opt. Express* **2015**, *23*, 1428−1437.

(16) Drevinskas, R.; Beresna, M.; Gecevičius, M.; Khenkin, M.; Kazanskii, A. G.; Matulaitienė, I.; Niaura, G.; Konkov, O. I.; Terukov, E. I.; Svirko, Y. P.; Kazansky, P. G. Giant Birefringence and Dichroism Induced by Ultrafast Laser Pulses in Hydrogenated Amorphous Silicon. *Appl. Phys. Lett.* **2015**, *106*, 171106.

(17) Drevinskas, R.; Beresna, M.; Zhang, J.; Kazanskii, A. G.; Kazansky, P. G. Ultrafast Laser-Induced Metasurfaces for Geometric Phase Manipulation. *Adv. Opt. Mater.* **2017**, *5*, 1600575.

(18) Song, J.; Dai, Y.; Tao, W.; Gong, M.; Ma, G.; Zhao, Q.; Qiu, J. Surface Birefringence of Self-Assembly Periodic Nanostructures Induced on 6H-SiC Surface by Femtosecond Laser. *Appl. Surf. Sci.* **2016**, *363*, 664−669.

(19) Ray, S.; Banerjee, R.; Basu, N.; Batabyal, A. K.; Barua, A. K. Properties of Tin Doped Indium Oxide Thin Films Prepared by Magnetron Sputtering. *J. Appl. Phys.* **1983**, *54*, 3497−3501.

(20) Hamberg, I.; Granqvist, C. G. Evaporated Sn-doped In 2 O 3 Films: Basic Optical Properties and Applications to Energy-efficient Windows. *J. Appl. Phys.* **1986**, *60*, R123−R160.

(21) Bonse, J.; Munz, M.; Sturm, H. Structure Formation on the Surface of Indium Phosphide Irradiated by Femtosecond Laser Pulses. *J. Appl. Phys.* **2005**, *97*, 013538.

(22) Costache, F.; Kouteva-Arguirova, S.; Reif, J. Sub-Damage-Threshold Femtosecond Laser Ablation from Crystalline Si: Surface Nanostructures and Phase Transformation. *Appl. Phys. A: Mater. Sci. Process.* **2004**, *79*, 1429−1432.

DOI: 10.1021/acsphotonics.7b01082
ACS Photonics 2017, 4, 2944−2951

(23) Dufft, D.; Rosenfeld, a.; Das, S. K.; Grunwald, R.; Bonse, J. Femtosecond Laser-Induced Periodic Surface Structures Revisited: A Comparative Study on ZnO. *J. Appl. Phys.* **2009**, *105*, 34908.
(24) Huang, M.; Zhao, F.; Cheng, Y.; Xu, N.; Xu, Z. Origin of Laser-Induced near-Subwavelength Ripples: Interference between Surface Plasmons and Incident Laser. *ACS Nano* **2009**, *3*, 4062−4070.
(25) Bonse, J.; Sturm, H.; Schmidt, D.; Kautek, W. Chemical, Morphological and Accumulation Phenomena in Ultrashort-Pulse Laser Ablation of TiN in Air. *Appl. Phys. A: Mater. Sci. Process.* **2000**, *71*, 657−665.
(26) Rudenko, A.; Colombier, J.-P.; Itina, T. E. From Random Inhomogeneities to Periodic Nanostructures Induced in Bulk Silica by Ultrashort Laser. *Phys. Rev. B: Condens. Matter Mater. Phys.* **2016**, *93*, 75427.
(27) Reif, J.; Costache, F.; Henyk, M.; Pandelov, S. V. Ripples Revisited: Non-Classical Morphology at the Bottom of Femtosecond Laser Ablation Craters in Transparent Dielectrics. *Appl. Surf. Sci.* **2002**, *197−198*, 891−895.
(28) Yariv, A.; Yhe, P. *Optical Waves in Crystals*; Wiley: New York, 1984.
(29) Born, M.; Wolf, E. *Principles of Optics*; Pergamon Press: Oxford, 1980.
(30) Kikuta, H.; Ohira, Y.; Iwata, K. Achromatic Quarter-Wave Plates Using the Dispersion of Form Birefringence. *Appl. Opt.* **1997**, *36*, 1566−1572.
(31) Abdulhalim, I. Simplified Optical Scatterometry for Periodic Nanoarrays in the near-Quasi-Static Limit. *Appl. Opt.* **2007**, *46*, 2219.
(32) Lumerical Solutions, Inc. http://www.lumerical.com/tcad-products/fdtd/.
(33) Moerland, R. J.; Hoogenboom, J. P. Subnanometer-Accuracy Optical Distance Ruler Based on Fluorescence Quenching by Transparent Conductors. *Optica* **2016**, *3*, 112.
(34) García-Vidal, F. J.; Lezec, H. J.; Ebbesen, T. W.; Martín-Moreno, L. Multiple Paths to Enhance Optical Transmission through a Single Subwavelength Slit. *Phys. Rev. Lett.* **2003**, *90*, 213901.
(35) Cerkauskaite, A.; Drevinskas, R.; Rybaltovskii, A. O.; Kazansky, P. G. Ultrafast Laser-Induced Birefringence in Various Porosity Silica Glasses: From Fused Silica to Aerogel. *Opt. Express* **2017**, *25*, 8011.
(36) Zhang, J.; Drevinskas, R.; Beresna, M.; Kazansky, P. G. Polarization Sensitive Anisotropic Structuring of Silicon by Ultrashort Light Pulses. *Appl. Phys. Lett.* **2015**, *107*, 41114.
(37) Bomzon, Z.; Kleiner, V.; Hasman, E. Pancharatnam−Berry Phase in Space-Variant Polarization-State Manipulations with Subwavelength Gratings. *Opt. Lett.* **2001**, *26*, 1424.
(38) Hasman, E.; Bomzon, Z.; Niv, A.; Biener, G.; Kleiner, V. Polarization Beam-Splitters and Optical Switches Based on Space-Variant Computer-Generated Subwavelength Quasi-Periodic Structures. *Opt. Commun.* **2002**, *209*, 45−54.
(39) Moreno, I.; Davis, J. A.; Hernandez, T. M.; Cottrell, D. M.; Sand, D. Complete Polarization Control of Light from a Liquid Crystal Spatial Light Modulator. *Opt. Express* **2012**, *20*, 364.
(40) Aharon, O.; Abdulhalim, I. Liquid Crystal Wavelength-Independent Continuous Polarization Rotator. *Opt. Eng.* **2010**, *49*, 34002.

DOI: 10.1021/acsphotonics.7b01082
ACS Photonics 2017, 4, 2944−2951